Mixture fraction analysis of combustion products in medium-scale pool fires

Ryan Falkenstein-Smith, Kunhyuk Sung, Jian Chen, Anthony Hamins*

National Institute of Standards and Technology, 100 Bureau Dr., Gaithersburg, MD 20899, United States of America

Abstract

A mixture fraction analysis is performed to investigate the characteristics of time-averaged gaseous species measurements made along the centerline of medium-scale pool fires steadily burning in a quiescent environment. A series of fire experiments are conducted using 30 cm diameter liquid and 37 cm diameter gas pool burners. All gaseous species measurements are extracted at various heights within the fire and analyzed using an Agilent 5977E Series Gas Chromatograph with mass selectivity and thermal conductivity detectors. Soot mass fractions are simultaneously measured during gas sampling. For all fuels, the results show that the local composition plotted as a function of mixture fraction collapses the experimental data into a few coherent lines that nearly match the idealized reactions. Differences between the theoretical and experimental data are attributed to the presence of carbon monoxide, soot, and other intermediate carbon-containing species. The ratio of carbon monoxide and soot is presented as a function of mixture fraction in which a trend is observed.

Keywords:

*Corresponding author: Anthony Hamins

Email address: anthony.hamins@nist.gov (Anthony Hamins)

Mixture fraction, Pool fires, Carbon-to-hydrogen ratio, Combustion products, Chemical composition

1. Introduction

Computational fluid dynamics (CFD) models are an important component of performance-based design in fire protection engineering. A requirement of their acceptance in the design process is that these models be verified and validated, the latter of which involves comparison with experimental measurements. The primary objective of this work is to provide data for use in fire model validation. Mixture fraction-based combustion analysis has been widely used to characterize combustion chemistry of different fire systems [1–5]. Comparison of species composition in terms of mixture fraction is convenient as it reveals the difference in the structure of fires burning different types of fuels at different scales.

In a pool fire, the fuel surface is isothermal, flat, and horizontal, providing a well-defined boundary condition for modeling. Fuel and product species concentrations and temperatures have a significant influence on the heat feedback to the fuel surface, which directly affects the burning rate. A zone of particular interest is the fuel-rich core between the flame and the pool surface, where gaseous species can absorb radiation that would otherwise have been transferred to the fuel surface. Few studies in the fire literature have reported local chemical species measurements within the envelope of medium-scale pool fires.

In this study, a mixture fraction analysis is performed to characterize the measured spatial distribution of the principal chemical species in pool fires steadily burning in a well-ventilated, quiescent environment. A series of fire experiments is conducted using a 30 cm diameter liquid and 37 cm diameter gas pool burner.

Gaseous species and soot measurements are made at various locations within the fire. The measurement techniques applied in this study are justified based on previous work in the fire literature [6, 7]. Four fuels are considered: methanol, ethanol, acetone, and methane. Through the analysis of the species composition at various locations within the fire, this study attempts to provide insight into the combustion chemistry of pool fires.

2. Description of experiments

2.1. Pool burner setup

All experiments are conducted under a canopy hood surrounded by a cubic enclosure, 2.5 m on a side, made of a double layer wire-mesh screen (5 mesh/cm) to reduce the impact of room ventilation. All measurements are made once the mass burning rate reaches a steady-state, achieved approximately 10 min and 2 min after ignition for the liquid and methane fuels, respectively.

Liquid fuels are burned in a circular, stainless-steel pan, made from cold-rolled steel, with an inner diameter of 30.1 cm, a depth of 15 cm, and a wall thickness of 1.3 mm. The liquid burner has an overflow basin, which extends 2.5 cm beyond the burner wall. Fuel to the liquid burner is gravity fed from a reservoir positioned on a mass load cell located outside the enclosure and is manually controlled by adjusting the fuel flow using a needle valve. The fuel surface is maintained 10 mm below the burner rim to match previous experimental conditions [8–11]. Methane is burned using a round 37 cm diameter, porous-metal burner. Fuel to the gas burner is controlled via a mass flow controller located outside of the enclosure. The bottoms of both burners are maintained at a constant temperature by flowing water ($20\ ^{\circ}\mathrm{C} \pm 3\ ^{\circ}\mathrm{C}$). Further descriptions of the liquid and gas burners are found

in Refs. [9, 12–15].

The mean flame height is estimated from 3600 frames of high-resolution video of the experiments using MATLAB's Image Processing Toolbox[1]. Imported color images are decomposed into binary (i.e., black and white) images using a pre-set threshold level. The flame height for a single frame is defined as the distance between the pool surface and the flame tip. All measurements are repeated, then averaged to provide the mean flame height.

2.2. Measuring the volume fraction of gaseous species

Gaseous species measurements are made using an Agilent 5977E Series Gas Chromatograph with mass selectivity and thermal conductivity detectors (GC/MSD). Figure 1 displays the flow diagram for gas sampling. The gases are extracted by a vacuum pump located downstream of the GC/MSD. Gas samples are collected using a quenching probe, which is composed of two concentric, stainless-steel tubes with outer annular coolant flow and inner, extracted sample flow. The inner and outer tube diameters are 8 mm and 16 mm, respectively. Water at approximately 90 °C flows through the sampling probe during sampling. The remainder of the sampling line leading into the GC/MSD is heated with electrical heating tape to approximately 140 °C to prevent condensation of water and liquid fuels within the line.

Depending on the probe location within the fire, the sampling period varies from 12 min to 25 min, ensuring a sufficient mass of soot and gas sample is col-

[1] Certain commercial products are identified in this report to specify adequately the equipment used. Such identification does not imply a recommendation by the National Institute of Standards and Technology, nor does it imply that this equipment is the best available for the purpose.

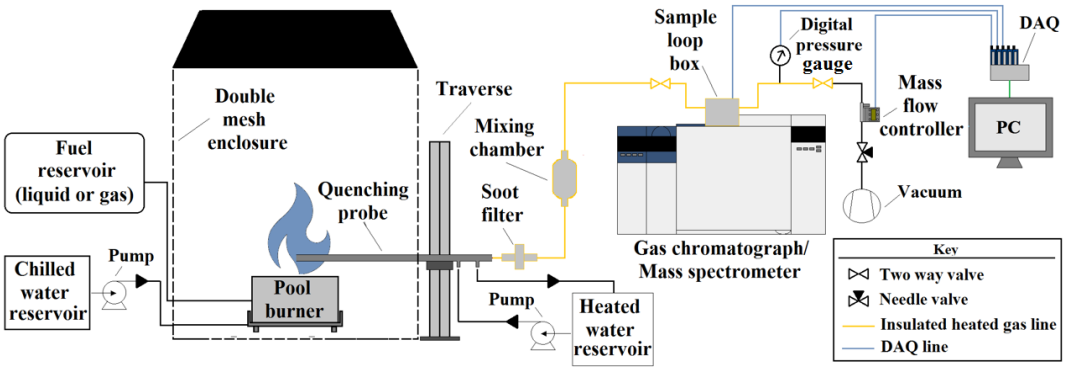

Figure 1: A schematic of the extractive sampling and analysis system.

lected. The flow is controlled using a mass flow controller (Alicat Scientific MC-Series) located in front of the vacuum pump within the sampling line. During the gas sampling procedure, the volumetric flow is approximately 200 mL/min and recorded at 2 Hz. All measurements using the GC/MSD are repeated at least twice at each location along the centerline of the pool fire. Gaseous species concentration measurements made at the same location are averaged. The mean mass fraction, $\bar{Y}_i$, of a given species i is calculated from the measured volume fraction, $\bar{X}_i$, using the following expression:

$$\bar{Y}_i = \frac{\bar{X}_i \mathrm{W}_i}{\sum \bar{X}_i \mathrm{W}_i} \tag{1}$$

where W_i is the molecular weight of a given species.

2.3. Centerline temperature measurements

Time-averaged temperature measurements are made along the centerline profiles of the pool fires at the same gas sampling locations. A S-type (Pt, 10% Rh/Pt), bare-wire, thermocouple (OMEGA P10R-001) with a 50 μm wire diameter and a bead diameter approximately 150 μm is used. Optical microscope measurements show that the thermocouple bead is spherical. The measurement and its

uncertainty are described in detail in Refs. [16, 17]. The flow field is unsteady, so thermal inertia effects are considered following Shaddix [18], in which conduction losses are assumed to be small, and digital compensation for thermal inertia is calculated using the Nusselt number, applying the Ranz-Mashall model [19]. The temperature-dependent gas properties for Re and Pr are taken as those of air , and the temperature-dependent emissivity and the thermophysical properties of platinum are taken from Refs. [20, 21]. Temperature measurements are sampled at 250 Hz for 2 min, or approximately 300 pulsing cycles [22].

2.4. Determining soot mass fraction

Soot mass fraction, Y_s, is measured using a well established gravimetric technique [7]. Soot is filtered out of the gas stream using a filter held in a stainless steel particulate filter holder (PALL 2220). Before an experiment, a desiccated 47 mm polytetrafluoroethylene (PTFE) filter is weighed and placed into its holder. The filter holder is positioned within the gas sampling line behind the quenching probe and heated with tape to approximately 140 °C to prevent condensation of water and liquid fuels on the filter. After sampling, the filter is removed and dried in a desiccator. After drying for 48 h, the filter's final weight is measured. Approximately 1 mg of soot is collected during the sampling period. The mass of the PTFE filter and cleaning patches are measured three times before and after each test. After most experiments, soot deposits are observed on the inner walls of the quenching probe. Dedicated gun cleaning patches (Hoppe's 9 1203S) are used to clean the inside of the quenching probe with no cleaning solvent. At least two patches are used to collect soot on the inside of the probe. A petri dish is placed below one end of the probe to catch dislodged soot and patches. Soot collection on the inside of the probe concludes once an applied patch is observed to have no

soot. Patches are weighed immediately before and 48 h after cleaning the inside of the probe. Significant secondary reactions are not expected to occur once the filter and pathches are exposed to ambient air. A brief investigation on the variation of weight measurements for multiple probe cleaning patches and over different periods was conducted and found no significant variation in the calculated mass fraction that would suggest a significant error in the approach.

The soot mass fraction, Y_s, is computed from the mass of the soot collected from the PTFE filter and gun cleaning patches, m_s, the ratio of the mass flow controller's temperature reading, T_∞, to the effective temperature of the gas obtained from the thermocouple measurements, T_g, the total mass of gas sampled, m_tot, based on the mass flow controller readings:

$$Y_\mathrm{s} = \frac{m_\mathrm{s} V_s}{\dot{V}\,\Delta t\, m_\mathrm{tot}} \frac{T_\infty}{T_\mathrm{g}} \tag{2}$$

where the total mass of gas sampled is represented by the product of the average volumetric flow rate measured by the mass flow controller, $\dot{V}$, the gas sampling time, Δt and the gas density. The gas density is represented by the ratio of total mass detected from the GC/MSD, m_tot and the injected sample volume, V_s.

2.5. Mixture fraction calculation

The mixture calculation follows the same approach as Ref. [23]. The mixture fraction, Z, is defined as the mass fraction of the gases containing carbon, including to soot, that originate in the fuel stream. It can be expressed as follows:

$$Z = \bar{Y}_\mathrm{F} + \frac{W_\mathrm{F}}{\mathrm{x}} \sum_{i \neq \mathrm{F}} \frac{\bar{Y}_i}{W_i} \tag{3}$$

where $\bar{Y}_\mathrm{F}$, W_F, and x are the mass fraction, molecular weight, and number of carbon atoms in the fuel molecule, respectively. Assuming ideal (i.e. no CO or soot),

infinitely-fast (fuel and oxygen from the air cannot co-exist) combustion, the mass fractions of all species can be expressed as piece-wise linear "state relations" according to the following reaction:

$$\begin{aligned} \mathrm{C_xH_yO_z} + \eta(\mathrm{x} + \frac{\mathrm{y}}{4} - \frac{\mathrm{z}}{2})\ (\mathrm{O_2} + 3.76\ \mathrm{N_2} + 0.0445\ \mathrm{Ar}) \rightarrow \\ \max(0, 1-\eta)\ \mathrm{C_xH_yO_z} + \max(0, 1-\eta)\ (\mathrm{x} + \frac{\mathrm{y}}{4} - \frac{\mathrm{z}}{2})\ \mathrm{O_2} \\ + \eta(\mathrm{x} + \frac{\mathrm{y}}{4} - \frac{\mathrm{z}}{2})\ (3.76\ \mathrm{N_2} + 0.0445\ \mathrm{Ar}) \\ + \min(1, \eta)\ \mathrm{x}\ \mathrm{CO_2} + \min(1, \eta)\ \frac{\mathrm{y}}{2}\ \mathrm{H_2O} \end{aligned} \quad (4)$$

The parameter η is the reciprocal of the local fuel equivalence ratio, ϕ,

$$\phi = \frac{(\mathrm{F/A})}{(\mathrm{F/A})_{\mathrm{st}}} = \frac{1}{\eta} \quad (5)$$

where $\mathrm{F/A}$ is the fuel-air mass ratio and the subscript st denotes the stoichiometric condition. The idealized mass fractions of the products are obtained from the right side of Eq. 4. The stoichiometric mixture fraction, Z_{st}, using the following expression:

$$Z_{\mathrm{st}} = \frac{W_{\mathrm{F}}}{W_{\mathrm{F}} + WA} \quad (6)$$

The calculated stoichiometric mixture fractions for the fuels investigated in this work are presented in Table 1.

2.6. Uncertainty analysis

An extensive uncertainty analysis of measurements is provided in Ref. [17]. The variance between repeated measurements is the most significant contributor to the uncertainties. The uncertainty of the mixture fraction is expressed as a function of the uncertainties in the carbon carrying species:

$$u_Z{}^2 = u_{\tilde{Y}_{\mathrm{F}}}{}^2 + \left(\frac{W_{\mathrm{F}}}{\mathrm{x}}\right)^2 \sum_{i \neq \mathrm{F}} \left(\frac{u_{\tilde{Y}_i}}{\mathrm{W}_i}\right)^2 \quad (7)$$

where u_Z is the combined uncertainty of the mixture fraction determined from the combined uncertainty of the mass fractions of all carbon carrying species. Unless otherwise stated, uncertainty in this work is expressed as the combined relative uncertainty with an expansion factor of two, representing a 95 % confidence level.

3. Results

3.1. Flame observations

The methanol fire is purely blue, whereas the ethanol, acetone, and methane fires are more luminous and yellow. The measured time-averaged burning rates and calculated ideal heat release rates are listed in Table 1. The heat release rates are calculated from the product of the mass burning flux and the idealized heat of combustion. The burning rate of the methane fire is set to match a value used in our previous study [24] that measured other fire characteristics. The methanol fire has the lowest average flame height, followed by the ethanol, methane, and acetone. The measured mean flame heights match Heskestad's correlation [25] to within measurement uncertainty. The measured flame heights are also within the uncertainty bounds of measurements made by Kim et al. [10].

3.2. Comparison of fire structure

Figure 2 displays the time-averaged gas temperatures as a function of the mixture fraction. The maximum mean temperature for each fuel peaks is close to their respective stoichiometric mixture fraction values. Methane has the highest peak mean temperature of 1350 K with methanol, ethanol, and acetone exhibiting maximum mean temperatures of 1316 K, 1281 K, and 1190 K, respectively. The methanol temperature profile is consistent with previous measurements [22].

Table 1: List of measurements and thermochemical properties of fuels burning in well-ventilated round pool fires

Parameter (units)	**Methanol**	**Ethanol**	**Acetone**	**Methane**
Burner Diameter (cm)	30.1	30.1	30.1	37.0
Mass Burning Flux (g/m^2s)	12.4 ± 1.1	13.9 ± 0.8	17.6 ± 2.7	6.4 ± 0.1
Idealized Heat Release Rate (kW)	17.4 ± 1.4	26.3 ± 1.5	35.5 ± 5.4	34.5 ± 0.5
Mean Flame Height (cm)	36 ± 16	61 ± 28	91 ± 34	64 ± 31
Z_{st}	0.13	0.10	0.09	0.05
Carbon/Hydrogen Ratio	1/4	1/3	1/2	1/4

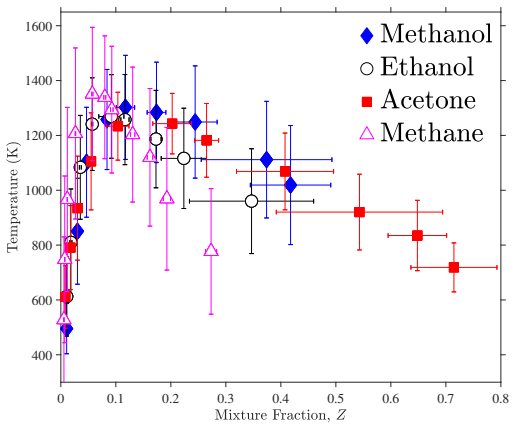

Figure 2: Mean and RMS centerline temperature as a function of the mixture fraction for the methanol, ethanol, acetone, and methane pool fires

Figure 3 shows the soot mass fraction as a function of mixture fraction for the ethanol, acetone, and methane pool fires. No soot is detected in the methanol fire. Acetone's soot mass fraction peaks in fuel-rich conditions whereas methane and ethanol peak close to stoichiometric conditions. In comparison, the acetone pool fire has a factor of 5 and 6 larger soot mass fraction than the ethanol and methane pool fires, respectively.

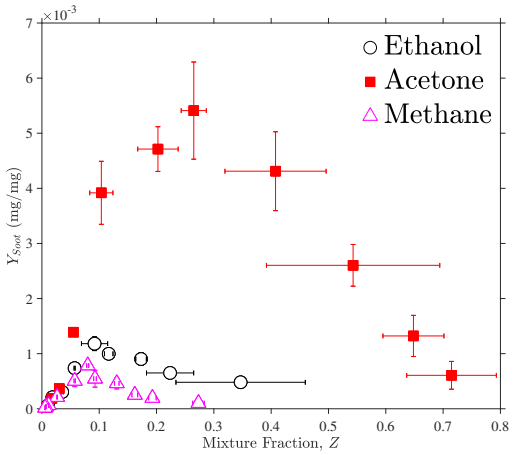

Figure 3: Soot mass fraction as a function of the mixture fraction for the ethanol, acetone, and methane pool fires. No soot is detected in the methanol fire.

3.3. Verifying gas species measurements

Major species detected in the TCD and MS include combustion reactants (fuels and oxygen, O_2), combustion products such as water, H_2O, and carbon dioxide, CO_2, combustion intermediates such as carbon monoxide, CO, hydrogen, H_2, and inert gases such as nitrogen, N_2, and argon, Ar. Methane is detected and quantified in all fires. In the case of the ethanol, acetone, and methane pool fires, soot, benzene, acetylene, ethylene, and ethane are also detected, which is consistent with previous literature [26, 27]. As a way to verify the accuracy of the experimental

method, the ratio of carbon to hydrogen atoms contained in all gaseous species is calculated at each vertical measurement location using the following function:

$$\frac{\mathrm{C}}{\mathrm{H}} = \frac{W_{\mathrm{C}}}{W_{\mathrm{H}}} \frac{\sum \mathrm{x}_i \bar{X}_i}{\sum \mathrm{y}_i \bar{X}_i} \tag{8}$$

where the summation is over all measured gaseous species, and x_i and y_i are the numbers of carbon and hydrogen atoms in the molecule, respectively. The carbon-to-hydrogen ratio of the parent fuel molecules are reported in Table 1. As seen in Fig. 4, the theoretical carbon-to-hydrogen ratio for each fuel, represented by the dotted lines, shows agreement with the gaseous species measurements within measurement uncertainty. The conservation of the carbon to hydrogen ratio at each position for each fuel also validates the experimental technique and suggests that the condensation of the condensable or semi-volatile species is minimal.

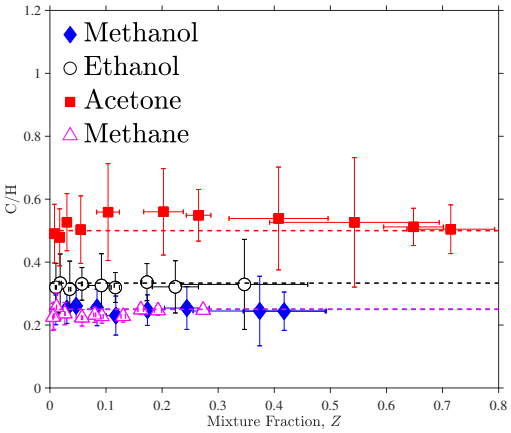

Figure 4: Carbon-to-hydrogen ratio as a function of the mixture fraction calculated from all measured gaseous species compared to the theoretical values for the four pool fires.

3.4. Mixture fraction analysis

Figure 5 shows the mean mass fraction measurements as a function of the mixture fraction for the methanol, ethanol, acetone, and methane pool fires, re-

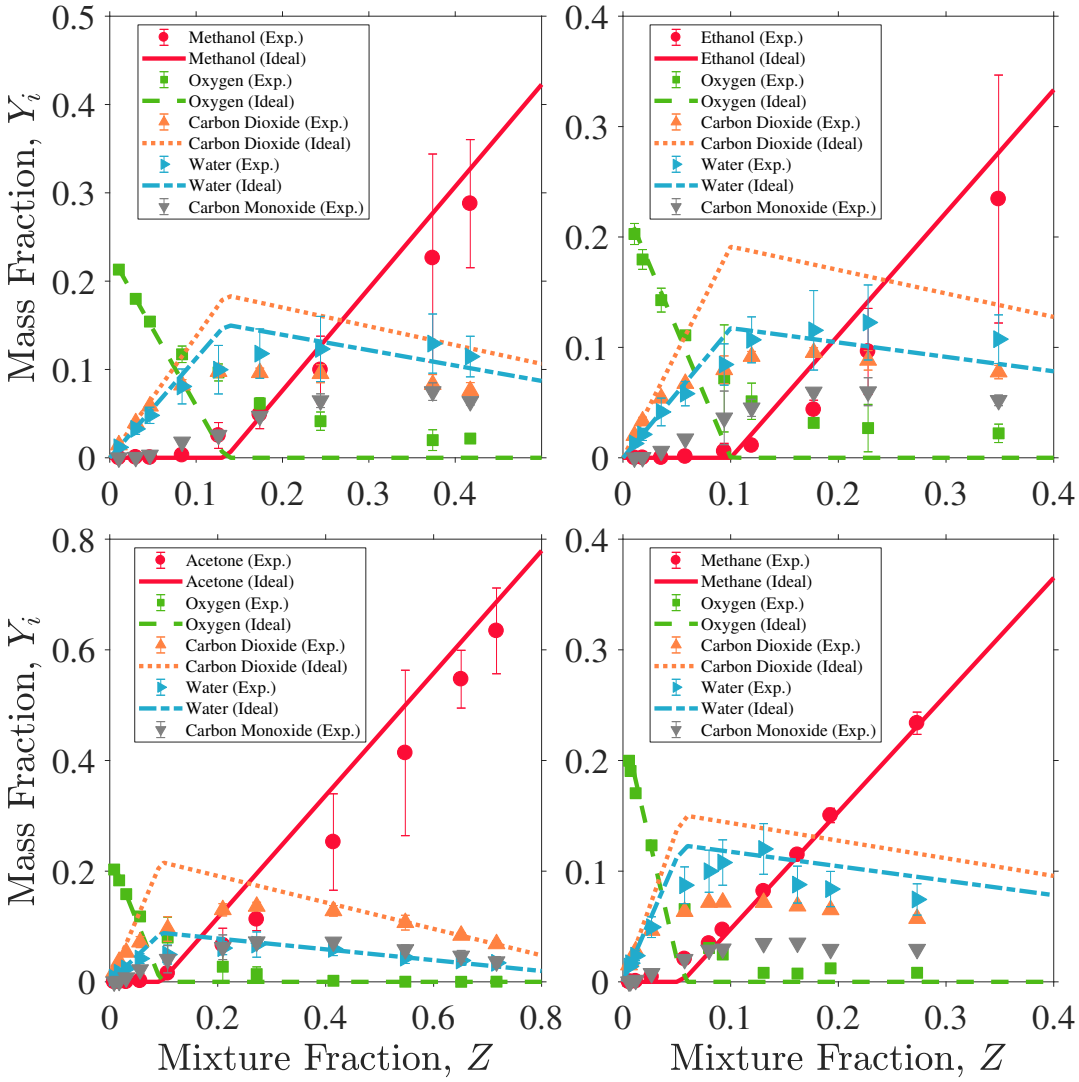

Figure 5: Mean mass fractions as a function of the mixture fraction for the methanol (top left), ethanol (top right), acetone (bottom left), and methane (bottom right) pool fires.

spectively. The combined expanded uncertainty of each measurement is also presented. The dotted lines represent ideal combustion from Eq. (4).

The stoichiometric conditions (see Table 1) can be seen near the intersection

of fuel and oxygen at $Y_i = 0$. Where the mixture fraction is much less than stoichiometric, all major gaseous species are in close agreement with the ideal state relations; the measured mass fractions of unburned fuel and CO are nearly zero, and the O_2 is close to its respective theoretical value. The measured mass fraction of CO_2 and H_2O are found to peak close to the stoichiometric mixture fraction. As the mixture fraction increases, the mass fraction of O_2 is nearly zero, whereas the mass fraction of each fuel increases linearly. In the fuel-rich region, the measured mass fraction of CO_2 differs considerably from the ideal state relation due to the substantial amount of CO and soot. This has been observed in other mixture fraction analyses and is attributed to finite rate chemistry effects associated with slow CO chemistry [5]. For the cases of the liquid pool fires, the over-shoot of fuel is likely linked to the presence of other intermediate carbon-containing species close to the fuel surface. This is exemplified in the fuel-rich region for acetone in which the fuel concentration is low while CO_2 is in fair agreement with the state relations; the larger portion of CO and soot, relative to other fuels, could account for the difference.

3.5. Carbon balance

The measurements show that the elemental carbon was primarily partitioned among CO_2, CO, CH_4, and soot. Other hydrocarbons, such as benzene, acetylene, ethylene, and ethane, were measured in trace/small quantities compared to CH_4. Figure 6 shows the mass ratio of CO to soot as a function of mixture fraction for the ethanol, acetone, and methane fires. The general trend of each fuel shows that the ratio of CO to soot exponentially decreases as the mixture fraction approaches fuel lean conditions. Köylü et al. [28] reported that the mass-based ratio of CO to soot generation factors in the overfire (i.e., the fuel-lean exhaust stream) region

of non-premixed hydrocarbon flames for a range of strongly sooting fuels was 0.34 ± 0.09. It is observed that the ratio of CO and soot tends to Köylü's value under fuel-lean conditions. However, the measurements made in this work are made within the fire, primarily below the flame tip, as opposed to the over fire region investigated by Köylü [28].

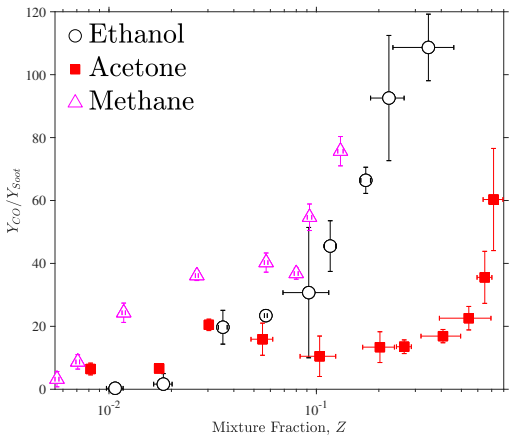

Figure 6: Mass based carbon monoxide to soot ratio as a function of the mixture fraction.

4. Conclusion

This study characterizes the structure of several medium-scale pool fires steadily burning in a quiescent environment. Temperature and soot centerline profiles for methanol, ethanol, acetone, and methane are reported. The calculated carbon-to-hydrogen ratio at each location is shown to be in agreement with the parent fuel values, which validates the accuracy of the measurements. Major species detected in the centerline profile of the pool fires are represented as a function of mixture fraction. As expected, carbon-containing species are shown to be less than the state relations in fuel-rich regions due to the presence of CO and soot. For

ethanol, acetone, and methane fires, the ratio of CO to soot is observed to decline when changing from fuel-rich to fuel-lean conditions. In the future, the technique described in this work will be applied for non-centerline position measurements and additional fuels. The expanded dataset will allow for additional comparisons between results and equilibrium values, which will aid in the development of various chemical sub-models for application in CFD fire models.

References

[1] R. Bilger, Reaction rates in diffusion flames, Combustion and Flame 30 (1977) 277–284.

[2] N. Peters, Laminar diffusion flamelet models in non-premixed turbulent combustion, Progress in Energy and Combustion Science 10 (3) (1984) 319–339.

[3] J. Floyd, C. Wieczorek, U. Vandsburger, Simulations of the virginia tech fire research laboratory using large eddy simulation with mixture fraction chemistry and finite volume radiative heat transfer, in: Proceedings of the Ninth International Interflam Conference. Interscience Communications, London, Vol. 12, 2001.

[4] A. Hamins, K. Seshadri, The structure of diffusion flames burning pure, binary, and ternary solutions of methanol, heptane, and toluene, Combustion and Flame 68 (3) (1987) 295–307.

[5] Y. Sivathanu, G. Faeth, Generalized state relationships for scalar properties in nonpremixed hydrocarbon/air flames, Combustion and Flame 82 (2) (1990) 211–230.

[6] E. L. Johnsson, M. F. Bundy, A. Hamins, Reduced-scale ventilation-limited enclosure fires-heat and combustion product measurements, in: Interflam Conference Proceedings, 2007, pp. 415–426.

[7] M. Choi, G. Mulholland, A. Hamins, T. Kashiwagi, Comparisons of the soot volume fraction using gravimetric and light extinction techniques, Combustion and Flame 102 (1-2) (1995) 161–169.

[8] S. Fischer, B. Hardouin-Duparc, W. Grosshandler, The structure and radiation of an ethanol pool fire, Combustion and Flame 70 (3) (1987) 291–306.

[9] A. Hamins, A. Lock, The Structure of a Moderate-Scale Methanol Pool Fire, NIST Technical Note 1928, National Institute of Standards and Technology, Gaithersburg, MD (2016).

[10] S. Kim, K. Lee, A. Hamins, Energy balance in medium-scale methanol, ethanol, and acetone pool fires, Fire Safety Journal 107 (2019) 44–53.

[11] E. Weckman, A. Strong, Experimental investigation of the turbulence structure of medium-scale methanol pool fires, Combustion and Flame 105 (1) (1996) 245–266.

[12] A. Hamins, S. Fischer, T. Kashiwagi, M. Klassen, J. Gore, Heat feedback to the fuel surface in pool fires, Combustion Science and Technology 97 (1-3) (1993) 37–62.

[13] A. Hamins, M. Klassen, J. Gore, T. Kashiwagi, Estimate of flame radiance via a single location measurement in liquid pool fires, Combustion and Flame 86 (3) (1991) 223–228.

[14] A. Hamins, T. Kashiwagi, R. R. Buch, Characteristics of pool fire burning, in: Fire Resistance of Industrial Fluids, ASTM International, 1996.

[15] A. Lock, M. Bundy, E. Johnsson, A. Hamins, G. Ko, C. Hwang, P. Fuss, R. Harris, Experimental Study of the Effects of Fuel Type, Fuel Distribution, and Vent Size on Full-Scale Underventilated Compartment Fires in an ISO 9705 Room, NIST Technical Note 1603, National Institute of Standards and Technology, Gaithersburg, MD (2008).

[16] K. Sung, J. Chen, M. Bundy, M. Fernandez, A. Hamins, The thermal character of a 1 m methanol pool fire, NIST Technical Note 2083, National Institute of Standards and Technology, Gaithersburg, MD (2020).

[17] R. Falkenstein-Smith, K. Sung, J. Chen, K. Harris, A. Hamins, The Structure of Medium-Scale Pool Fires, NIST Technical Note 2082, National Institute of Standards and Technology, Gaithersburg, MD (2020).

[18] C. Shaddix, Correcting thermocouple measurements for radiation loss: a critical review, Tech. Rep. CONF-990805, Sandia National Laboratories (1999).

[19] W. Ranz, W. Marshall, Evaporation from drops, Chem. eng. prog 48 (3) (1952) 141–146.

[20] DIPPR®, Design Institute for Physical Properties (DIPPR 801) (June 2019).

[21] F. Jaeger, E. Rosenbohm, The exact formulae for the true and mean specific heats of platinum between 0 and 1600 C, Physica 6 (7-12) (1939) 1123–1125.

[22] Z. Wang, W. Tam, K. Lee, J. Chen, A. Hamins, Thin filament pyrometry field measurements in a medium-scale pool fire, Fire Technology 56 (2) (2020) 837–861.

[23] G. H. Ko, A. Hamins, M. Bundy, E. L. Johnsson, S. C. Kim, D. B. Lenhert, Mixture fraction analysis of combustion products in the upper layer of reduced-scale compartment fires, Combustion and Flame 156 (2) (2009) 467–476.

[24] A. Hamins, K. Konishi, P. Borthwick, T. Kashiwagi, Global properties of gaseous pool fires, in: Symposium (International) on Combustion, Vol. 26, Elsevier, 1996, pp. 1429–1436.

[25] G. Heskestad, Luminous heights of turbulent diffusion flames, Fire Safety Journal 5 (2) (1983) 103–108.

[26] J. Gong, S. Zhang, Y. Cheng, Z. Huang, C. Tang, J. Zhang, A comparative study of n-propanol, propanal, acetone, and propane combustion in laminar flames, Proceedings of the Combustion Institute 35 (1) (2015) 795–801.

[27] S. Pichon, G. Black, N. Chaumeix, M. Yahyaoui, J. Simmie, H. Curran, R. Donohue, The combustion chemistry of a fuel tracer: Measured flame speeds and ignition delays and a detailed chemical kinetic model for the oxidation of acetone, Combustion and Flame 156 (2) (2009) 494–504.

[28] Ü. Ö. Köylü, G. M. Faeth, Carbon monoxide and soot emissions from liquid-fueled buoyant turbulent diffusion flames, Combustion and Flame 87 (1) (1991) 61–76.